Pergamon

*Chaos, Solitons & Fractals* Vol. 9, No. 8, pp. 1409–1428, 1998

Printed in Great Britain
0960–0779/98 $19.00 + 0.00

PII: S0960-0779(98)00073-3

# Experimental and Numerical Analysis of Nonlinear Phenomena in a Stochastically Excited Beam System with Impact

N. VAN DE WOUW, H. L. A. VAN DEN BOSCH, A. DE KRAKER, D. H. VAN CAMPEN

*Eindhoven University of Technology, Department of Mechanical Engineering, P.O. Box* 513, 5600 *MB Eindhoven, The Netherlands*

*(Accepted 24 February 1998)*

**Abstract**—The response of strongly nonlinear dynamic systems to stochastic excitation exhibits many interesting characteristics. In this paper, a strongly nonlinear beam-impact system under broad and small banded, Gaussian noise excitations is investigated. The response of this system is investigated numerically as well as experimentally. The emphasis lies on frequency domain characteristics. Phenomena like multiple resonance frequencies and stochastic equivalents of harmonic and subharmonic solutions are found. Improved understanding of these stochastic response characteristics is obtained by comparing them to nonlinear periodic response features of the system. It is shown that these stochastic response phenomena can provide information on the periodic response characteristics of the system. The observed stochastic characteristics have more general value and meaning than mere application to this system suggests. © 1998 Elsevier Science Ltd. All rights reserved.

## 1. INTRODUCTION

Nonlinear dynamic systems forced by random processes are often encountered in practice. The source of randomness can vary from surface randomness in vehicle motion, environmental changes, such as earthquakes and wind exciting high rise buildings or wave motions at sea exciting offshore structures or ships, to electric or acoustic noise exciting mechanical structures.

In this paper, a base excited beam system with a nonlinear elastic stop is investigated. Systems with elastic stops (typical examples of local non-linearities) represent a wide range of practical nonlinear dynamic systems. Examples are gear rattle, ships colliding against fenders and snubbers in solar panels on satellites. Although the nonlinearity is local, the dynamic behaviour of the entire system is influenced by it. Nonlinear periodic response phenomena of these kind of systems have been studied extensively, see [1–4].

When stochastic excitations are applied to the nonlinear beam system, it features many interesting, stochastic, nonlinear response phenomena. These phenomena are of specific interest because they shed light on the common characteristics of periodic and stochastic dynamic behaviour. As a consequence, the system's behaviour can be understood more thoroughly. The stochastic nonlinear response phenomena will be studied numerically as well as experimentally. The stochastic excitations will have a limited frequency band power spectral density. Still, these excitations can be broad band or narrow band processes. For strong, discontinuous nonlinearities, like an elastic stop, and band limited noise excitations, numerical integration is the only method

that provides accurate response information. Particularly, the nonlinear phenomena in the power spectral density of the response will be investigated extensively.

In the next section, Section 2, we introduce the nonlinear dynamic system and its model. In Section 3, a brief survey of simulated periodic response characteristics will be given. In Section 4, the simulation approach will be discussed. The simulation results will be presented in Section 5. In Section 6, we present the experimental set-up. Furthermore, in Section 7, the results of the experiments will be discussed and compared to simulation results, using identical excitations. Finally, in Section 8, we present some conclusions.

## 2. THE NONLINEAR BEAM SYSTEM

### *2.1. System description*

The nonlinear dynamic system comprises a linear elastic beam, which is clamped onto a rigid frame, and an elastic stop, see Fig. 1. The elastic stop consists of two half spheres. Moreover, Fig. 1 shows that the system is excited by a prescribed stochastic displacement $y$ of the rigid frame. The response $x$ is the vertical displacement of the beam at the point of contact. Firstly, in subsection Section 2.2, the elastic beam will be modeled. Secondly, in subsection Section 2.3, a model for the elastic stop will be presented. For both model components the estimation of their parameters is based on experiments and will be elucidated in these subsections. Finally, in subsection Section 2.4, a single-degree-of-freedom (SDOF) model of the above beam system will be specified.

### *2.2. Modeling the elastic beam*

The elastic beam is a continuum with an infinite number of degrees of freedom. Only transverse vibrations of the beam will be considered. Approximate spatially discretized models for continuous systems can be derived using the Rayleigh–Ritz method. The model used in this paper is a SDOF model, see Fig. 2:

$$m\ddot{x}+b\dot{x}+kx=F \tag{1}$$

where $x$ is the vertical displacement of the beam at the axial position $L$. The parameters $m$, $b$, and $k$ represent the mass, damping, and stiffness of the SDOF model, respectively. These model parameters are estimated by means of experiments carried out on the linear beam system. The parameters $m$ and $k$ are related to the lowest eigenfrequency of the linear beam. The damping parameter $b$ was chosen to properly represent the damping in the first and higher eigenmodes.

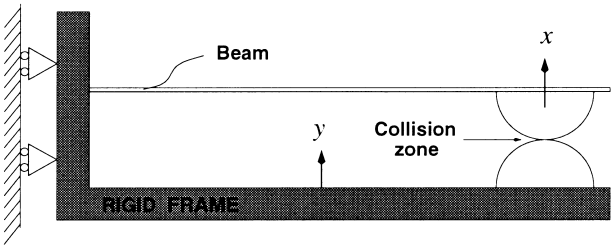


Fig. 1. The nonlinear base excited beam system.

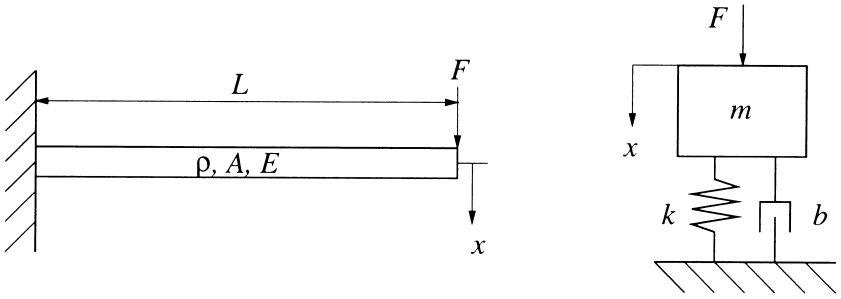


Fig. 2. The linear, stainless steel, beam system (left) with Young's modulus $E=2.1\ 10^{11}\,\mathrm{N/mm^2}$, density $\rho=7800\,\mathrm{kg/m^3}$, cross-section $A=59.6\,\mathrm{mm^2}$ and length $L=259.4\,\mathrm{mm}$ and its equivalent SDOF discrete model (right) with model parameters $m=37.75\ 10^{-3}\,\mathrm{kg}$, $k=736.3\,\mathrm{N/m}$ and $b=0.16\,\mathrm{kg/s}$.

### 2.3. *Modeling the elastic stop*

The elastic stop is modeled using a Hertzian contact model [5, 6]. Using the Hertzian model, the following relationship holds between the contact force $F$ and the relative displacement of the two colliding spheres $\delta=y-x$:

$$F=\frac{2}{3}E_r\sqrt{R_r}\delta^{1.5}=K_{\mathrm{Hertz}}\delta^{1.5}\quad\text{for}\quad\delta\geqslant 0 \tag{2}$$

In eqn (2), the reduced Young's modulus $E_r$ represents the material properties of both colliding bodies. Furthermore, the reduced radius of curvature $R_r$ represents the geometrical properties of the colliding bodies. These parameters are defined as:

$$E_r=\frac{2}{\dfrac{1-\upsilon_1^2}{E_1}+\dfrac{1-\upsilon_2^2}{E_2}},\quad R_r=\frac{R_1R_2}{R_1+R_2} \tag{3}$$

where $R_i$ is the principal radius of curvature of body $i$, while $E_i$ is the Young's modulus of body $i$ and $\upsilon_i$ the Poisson's ratio of body $i$. Since the collision phenomenon is generally quite complex, the following assumptions are made to validate eqn (2):

- The contact area is small compared to the geometry of the colliding bodies.
- The contact areas are perfectly smooth, so there is no friction between the colliding bodies.
- The material is isotropic and linearly elastic, so no plastic deformation occurs.
- The contact time is long enough to establish a quasi-static state.

Furthermore, it should be noted that eqn (2) still holds with significant deviation from the assumptions [7]. The parameter $K_{\mathrm{Hertz}}$ was determined experimentally ($K_{\mathrm{Hertz}}=2.1\ 10^8\,\mathrm{N/m^{1.5}}$).

The contact model (2) can be refined by adding a hysteretic damping term [8], accounting for energy loss during collision. The inclusion of hysteretic damping alters eqn (2) to:

$$F=K_{\mathrm{Hertz}}\delta^{1.5}\left(1+\frac{\mu}{K_{\mathrm{Hertz}}}\dot{\delta}\right)=K_{\mathrm{Hertz}}\delta^{1.5}\left[1+\frac{3(1-e^2)}{4}\frac{\dot{\delta}}{\dot{\delta}^-}\right]\quad\text{for}\quad\delta\geqslant 0 \tag{4}$$

in which $e$ is the coefficient of restitution, a geometry and material dependent measure for energy dissipation. Moreover, $\dot{\delta}^-$ represents the velocity difference of the two colliding bodies at the beginning of the collision. The coefficient of restitution $e$ is also estimated by means of experiments ($e=0.5$). The fact that $e$ differs significantly from 1 indicates that restitution should be added to

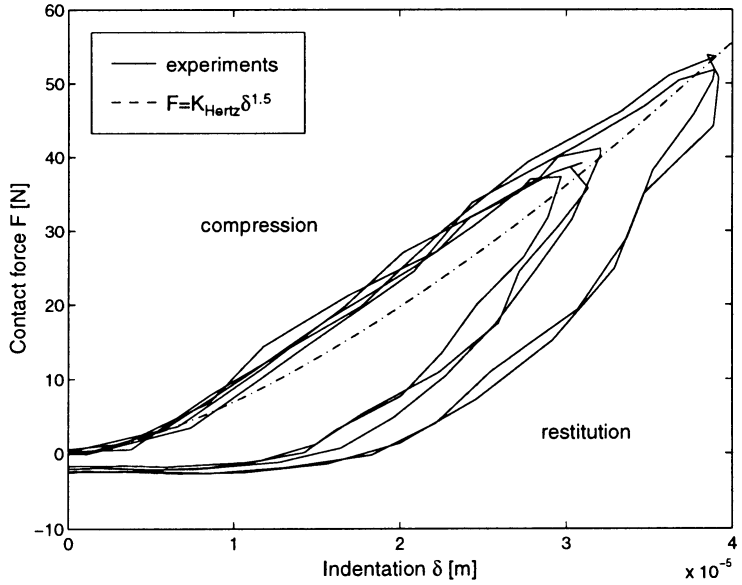


Fig. 3. Measurement of several collisions to estimate $K_{\text{Hertz}}$ and $e$.

the model. Both $K_{\text{Hertz}}$ as well as $e$ were estimated by means of a single experiment. In this experiment several collisions were observed. This resulted in information regarding the indentation $\delta$, the indentation velocity $\dot{\delta}$, and the contact force $F$. The dependency of the contact force $F$ between the colliding half spheres on the indentation $\delta$ is visualized in Fig. 3. The parameter $K_{\text{Hertz}}$ can be estimated by comparing the contact force $F$ and the indentation $\delta$ at maximum indentation ($\dot{\delta}=0$), assuming that the static contact force is proportional to $\delta^{1.5}$, see eqn (2). The coefficient of restitution $e$ can be estimated by considering the amount of energy loss $\Delta T$ during a collision. $\Delta T$ is equal to the surface within the hysteresis loop:

$$\Delta T = \oint \mu \delta^{1.5} \dot{\delta} d\delta \tag{5}$$

Therefore, $\mu$ can be estimated from:

$$\mu = \frac{\Delta T}{\oint \delta^{1.5} \dot{\delta} d\delta} \tag{6}$$

The coefficient of restitution can now be obtained from:

$$e = \sqrt{1 - \frac{\frac{4}{3}\mu \dot{\delta}^{-}}{K_{\text{Hertz}}}} \tag{7}$$

Both $K_{\text{Hertz}}$ and $e$ are least-squares estimates in which the information obtained from several collisions is accounted for.

### *2.4. The SDOF nonlinear dynamical model*

In the previous two subsections (Section 2.3 and Section 2.2), the two components of the beam system, namely, the beam and the elastic stop, were discussed. The assembled nonlinear model is visualized in Fig. 4 and its SDOF equation of motion becomes:

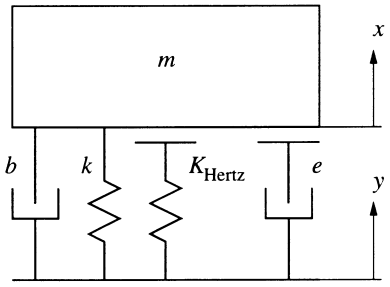


Fig. 4. The SDOF model for the nonlinear beam system.

$$m\ddot{x}+b\dot{x}+kx+\varepsilon(x-y)K_{\text{Hertz}}(x-y)^{1.5}\left[1+\frac{3(1-e^2)}{4}\frac{\dot{\delta}}{\dot{\delta}^-}\right]=b\dot{y}+ky \tag{8}$$

with:

$$\varepsilon(x-y)=\begin{cases}0 & \text{for} \quad x-y>0\\ 1 & \text{for} \quad x-y\leqslant 0\end{cases} \tag{9}$$

This model can now be used to simulate (through numerical time integration) the nonlinear response $x$ for different excitation forms $y$. The fact that $K_{\text{Hertz}}$ considerably exceeds $k$ in some sense indicates that the system is highly nonlinear.

## 3. SURVEY OF SIMULATED RESPONSE TO PERIODIC EXCITATION

In order to enlarge the ability to interpret the stochastic response phenomena, discussed later on in this paper, we present some periodic response phenomena of the nonlinear beam system. Figure 5 elucidates the dependency of the maximum absolute displacements $x$ occurring in the

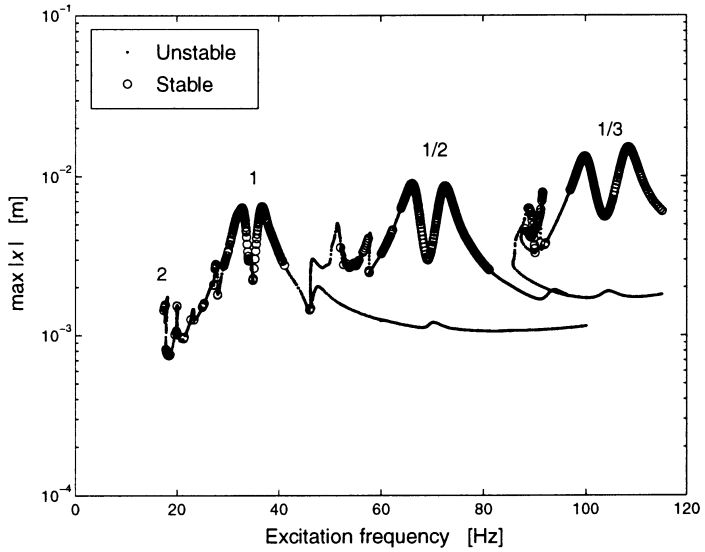


Fig. 5. Maximum absolute displacements max|$x$| of periodic solutions of a 4-DOF model [3].

simulated periodic solutions on the excitation frequency of the harmonic excitation, see Van de Vorst [3]. The system parameters used by Van de Vorst [3] were slightly different from those used in the stochastic simulations that follow. However, the main response characteristics are equivalent. Furthermore, the model used in the simulations by Van de Vorst [3] was a 4-DOF model. Some very important nonlinear response characteristics can be extracted from Fig. 5. Firstly, besides harmonic resonances, indicated by 1, subharmonic resonances appear, indicated by 1/2 and 1/3. Furthermore, a superharmonic resonance is indicated by 2. Secondly, a remarkable feature can be found in the fact that the maximum absolute values of the subharmonic solutions are higher than those of the harmonic solutions. Finally, all the resonance peaks are split into two separate peaks. This phenomenon can be related to the contribution of higher modes to the nonlinear response, and thus it will not appear using the SDOF model.

## 4. SIMULATION APPROACH

### *4.1. Generation excitation signals*

As mentioned before, the excitation form applied to the nonlinear beam system is Gaussian band limited noise. The form of the power spectral density of such an excitation process $y(t)$ is shown in Fig. 6. Obviously, $y(t)$ does not contain infinitely high frequencies, in contrast with white noise excitations. The energy contained by $y(t)$ is concentrated within a frequency band limited by $f_{\min}$ and $f_{\max}$. Therefore, differential eqn (8) can be solved numerically using classical (deterministic) integration techniques.

For a specific (desired) power spectral density function $P_{yy}(f)$ of the excitation process, one can simulate realizations of that Gaussian random process by using a method developed by Shinozuka [9] and Yang [10]. The idea behind this method is that a one-dimensional Gaussian random process $y(t)$ with zero mean and a one-sided power spectral density $P_{yy}(f)$ (frequency $f$) can be represented by a sum of cosine functions with a uniformly distributed random phase $\Phi$. A realization $\bar{y}(t)$ of $y(t)$ can be simulated by:

$$\bar{y}(t) = \sqrt{\Delta f}\,\mathrm{Re}\{F(t)\} \tag{10}$$

in which $\mathrm{Re}\{F(t)\}$ is the real part of $F(t)$ and

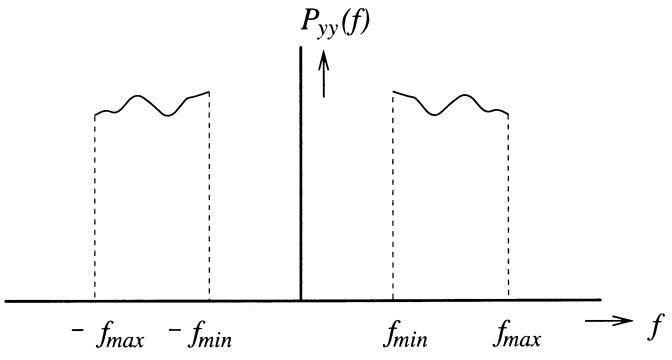


Fig. 6. Desired form of the power spectral density $P_{yy}(f)$ of excitation $y(t)$.

$$F(t)=\sum_{k=1}^{N}\left\{\sqrt{2P_{yy}(f_k)}\,\mathrm{e}^{i\phi_k}\right\}\mathrm{e}^{i2\pi f_k t} \tag{11}$$

is the finite complex Fourier transform of

$$\sqrt{2P_{yy}(f)}\;\mathrm{e}^{i\phi} \tag{12}$$

where $\phi$ are the realized values of $\Phi$.

### 4.2. Numerical time integration

Numerical time integration is used to compute time series of the response $x(t)$. The computed realizations of the response can be used to estimate the invariant measures of the stationary solutions, such as statistical moments, probability density function and power spectral density. For non-stationary responses many computationally expensive simulations would have to be executed in order to ensure an accurate estimate of the invariant measures at each point of time. However, the necessity of a large number of records can be eliminated when the response is stationary, as is the case here. In this case ergodicity with respect to a particular statistical moment can be assumed. This assumption allows the determination of the specific ensemble statistical moment by using its temporal counterpart.

The accuracy of the estimates of the stochastic invariants depends on the length (corresponding to a statistical error) and the integration accuracy underlying the time series. Therefore, the efficiency of the integration technique is an important issue. Variable step size schemes, in which stability checks and accuracy checks are performed each integration step, are rather inefficient with respect to our purpose. Therefore, a constant step size, second-order Runge–Kutta scheme is used. Higher-order schemes do not improve the order of convergence. This is a consequence of the fact that higher-order derivatives of the function $\underline{f}$ in the equations of motion in the state space formulation

$$\underline{f}(\underline{x},t)=\begin{bmatrix}\dot{x}\\ \ddot{x}\end{bmatrix}=\begin{bmatrix}\dot{x}_1\\ \dot{x}_2\end{bmatrix}$$

$$=\begin{bmatrix}x_2\\ -\dfrac{b}{m}x_2-\dfrac{k}{m}x_1-\varepsilon(x_1-y)K_{\mathrm{m}}^{\mathrm{Hertz}}(x_1-y)^{1.5}\left[1+\dfrac{3(1-e^2)}{4}\dfrac{\dot{\delta}}{\dot{\delta}^-}\right]+\dfrac{b}{m}\dot{y}+\dfrac{k}{m}y\end{bmatrix} \tag{13}$$

do not exist in the entire state space for systems with stops. Since explicit integration schemes are only conditionally stable, a minimum step size (that ensures stability) can be determined. Due to the major difference in stiffness between contact and non-contact situations, the minimal step sizes for these situations differ enormously. It would be very inefficient to choose one single constant step-size based on contact situations. Therefore, two different stable step-sizes are used. Of course, the step-sizes are adjusted to match accuracy conditions. Consequently, the time of impact has to be determined to avoid entering contact with the large integration time step. For this purpose the Hénon method [11] is implemented within the integration routine.

### 4.3. The Hénon method

The Hénon method [11] is a method to determine the time of impact. Here, the Hénon method means rearranging eqn (13) without the nonlinearities in such a way that $x_1-y$ becomes the

independent variable whereas $t$ becomes one of the dependent variables. The nonlinear part is superfluous, because the last time interval before the impact is observed. This results in:

$$\begin{bmatrix} \dfrac{\mathrm{d}t}{\mathrm{d}(x_1-y)} \\ \dfrac{\mathrm{d}x_2}{\mathrm{d}(x_1-y)} \end{bmatrix} = \begin{bmatrix} \dfrac{1}{x_2-\dot{y}} \\ \dfrac{1}{x_2-\dot{y}}\left(-\dfrac{b}{m}x_2-\dfrac{k}{m}x_1+2\dfrac{b}{m}\dot{y}+y\right) \end{bmatrix} \tag{14}$$

At the last time step before impact, this equation is integrated until $x_1-y=0$. This integration step results in the known variables $t_{\text{contact}}$, $x_2$ ($t_{\text{contact}}$) and $x_1(t_{\text{contact}})=y(t_{\text{contact}})$. Then a switch is made to a small integration step-size, for solving eqn (13), continuing at $t_{\text{contact}}$.

## 5. SIMULATION RESULTS

### *5.1. Broad band excitation*

In this subsection, the results of the simulations are presented. The target spectrum is taken uniformly distributed within a limited frequency band.

Firstly, a 0–200 Hz band excitation is applied to the system. The 0–200 Hz band excitation represents a broad band excitation, relatively to the response characteristics depicted in Fig. 5. In Fig. 7, the power spectral density of $y(t)$ is shown. The relative displacement of the two spheres, $\delta=y-x$, will also be used as a response variable in the presentation of the results. The probability density function (PDF) of the excitation, $y(t)$, is shown in Fig. 8. The excitation is Gaussian by the nature of its generation. An important property of the nonlinear response to Gaussian excitation is the fact that it is non-Gaussian. To illustrate this nonlinear response property, in Fig. 9, the probability density function of the response variable $\delta$ is shown. The fact that the response is non-Gaussian is also indicated by higher-order moments like skewness and kurtosis. The estimates for the skewness and kurtosis, which are defined by

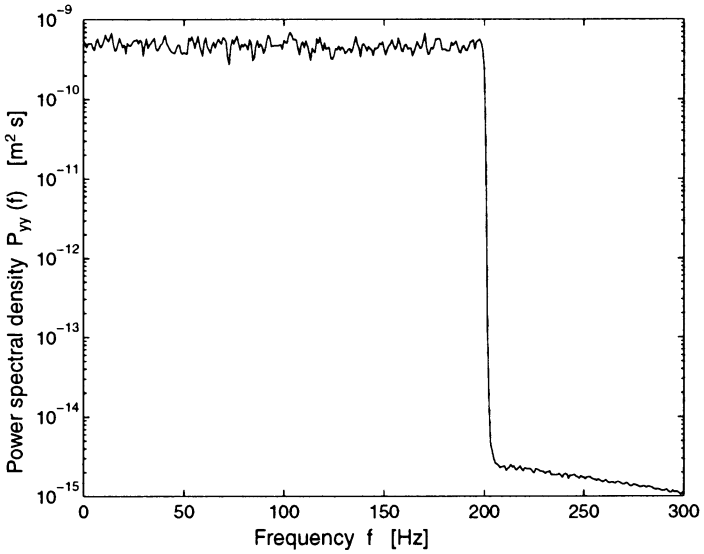


Fig. 7. Power spectral density of a 0–200 Hz band excitation $y(t)$.

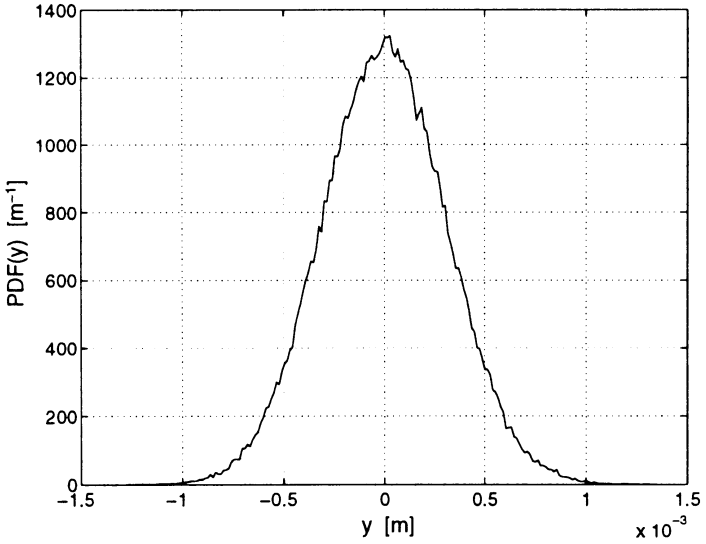


Fig. 8. Probability density function of the 0–200 Hz band excitation $y(t)$.

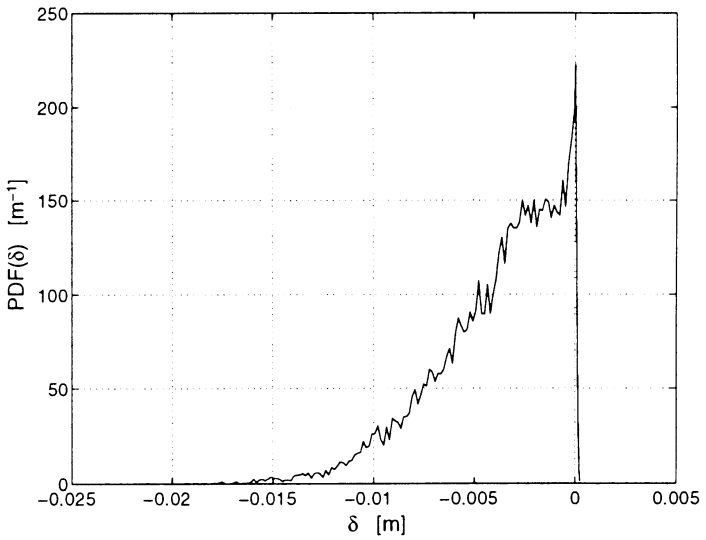


Fig. 9. Probability density function of $\delta(t)$ for a 0–200 Hz band excitation.

$$\hat{\gamma}_\delta = \frac{\Sigma(\delta_i - \bar{\delta})^3}{(n-1)\hat{\sigma}_\delta^3} \quad \text{and} \quad \hat{\kappa}_\delta = \frac{\Sigma(\delta_i - \bar{\delta})^4}{(n-1)\hat{\sigma}_\delta^4} \tag{15}$$

are $\hat{\gamma}_\delta = -1.02$ and $\hat{\kappa}_\delta = 3.96$ and thus deviate considerably from the Gaussian values $\gamma = 0$ and $\kappa = 3$. As far as the skewness is concerned, a deviation from zero points at an asymmetry of the probability density function. This asymmetry of the response is a nonlinear characteristic of the system due to the elastic stop, see Figs 10 and 11. To give a decisive answer as to whether a time series stems from a non-Gaussian process, the significance test of Shapiro and Wilk can be

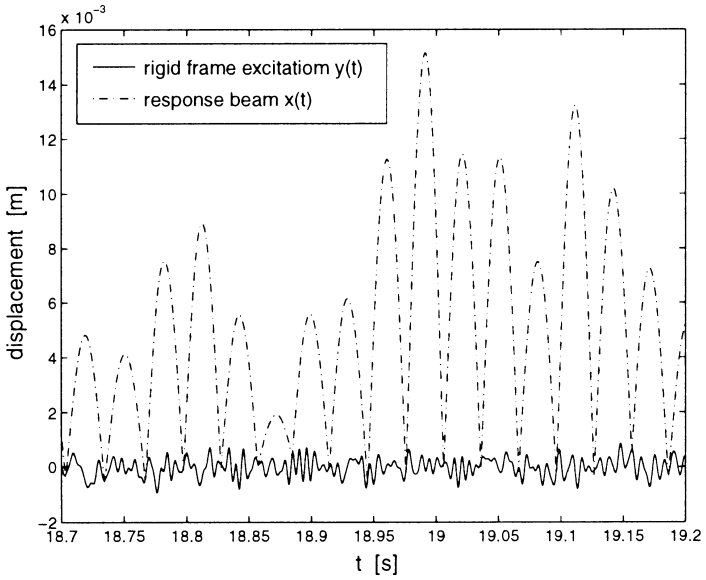


Fig. 10. Parts of time series: 200 Hz band excitation $y(t)$ and response beam $x(t)$.

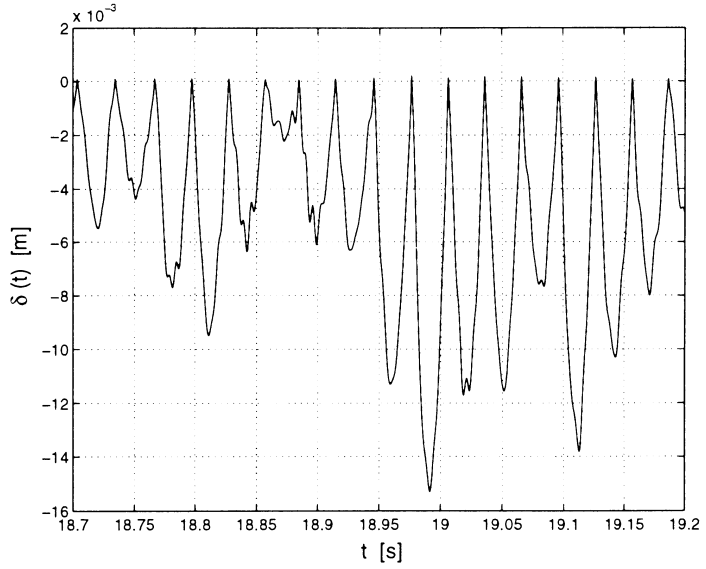


Fig. 11. Part of time-series $\delta(t) = y(t) - x(t)$.

performed. This test was specifically designed to suit this purpose. Of course, a test on the response variable $\delta(t)$ confirmed that it is definitely non-Gaussian.

In literature little attention has been paid to frequency domain characteristics of nonlinear dynamic systems excited by stochastic processes. Therefore, we will particularly focus on the observation and interpretation of these stochastic response phenomena. One-sided power spectral

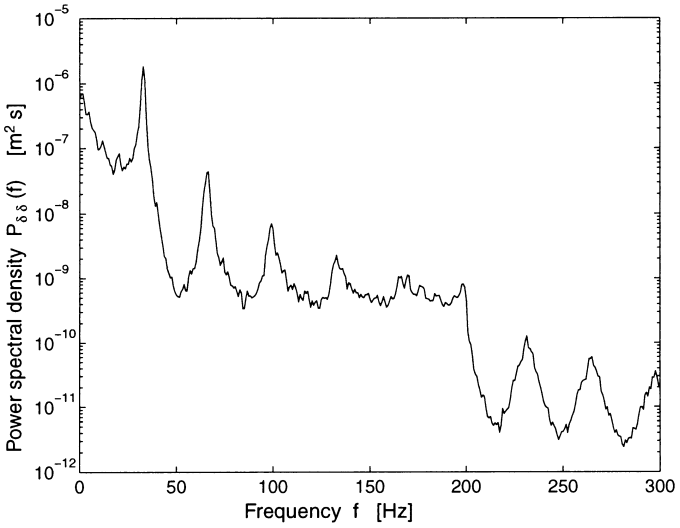


Fig. 12. Power spectral density of $\delta(t)$ for a 0–200 Hz band excitation.

densities will be considered throughout this paper. The power spectral density of the response variable $\delta(t)$ is shown in Fig. 12, which admits two important observations:

1. The power spectral density $P_{\delta\delta}(f)$ exhibits multiple resonance peaks.
2. The response signal contains a large amount of energy at low frequencies (0–15 Hz).

The second observation can be explained by the following reasoning. Due to the nonlinearity of the system, the frequencies in the response 'interact'. It is well-known that when the excitation, and therefore the response, contains two frequencies $f_1$ and $f_2$, the response can also contain the frequency $f_2 - f_1$ when the system is nonlinear. This 'difference'-frequency appears in the response as a consequence of the asymmetry of the nonlinear solution. Note that broad-band excitation contains a large number of nearby frequencies. Hence, a lot of interaction can be expected in this case. When those excitation frequencies lie in a resonance peak of the system, these 'difference'-frequencies will contain a significant amount of energy.

### 5.2. *Narrow band excitation*

In order to investigate which frequencies in the excitation are mainly responsible for the response phenomena mentioned above, four different smaller band excitations are applied:

1. A limited band excitation between $f_{\min} = 23$ Hz and $f_{\max} = 43$ Hz that covers the major part of the harmonic resonance peak.
2. A limited band excitation between $f_{\min} = 43$ Hz and $f_{\max} = 56$ Hz that lies in between the harmonic resonance peak and the 1/2 subharmonic resonance peak.
3. A limited band excitation between $f_{\min} = 56$ Hz and $f_{\max} = 76$ Hz that covers the major part of the 1/2 subharmonic resonance peak.
4. A limited band excitation between $f_{\min} = 89$ Hz and $f_{\max} = 109$ Hz that covers the major part of the 1/3 subharmonic resonance peak.

For these excitations the results regarding the power spectral density of the responses are depicted in Fig. 13, Fig. 14 and Fig. 15. Note that the 'harmonic' solution of a nonlinear system to harmonic excitation with frequency $f_e$ has a specific period time $1/f_e$ but comprises multiple frequencies ($f_e$, $2f_e$, $3f_e$,...). Clearly, this is also the case for stochastically excited systems, see Fig. 13. Furthermore, a band limited excitation between $f_{\min} = 43$ Hz and $f_{\max} = 56$ Hz is applied. The power spectral density of the response to this excitation is also shown in Fig. 13. The power spectral density of the response for an excitation frequency band of $23\,\text{Hz} \leqslant f_e \leqslant 43\,\text{Hz}$ shows a

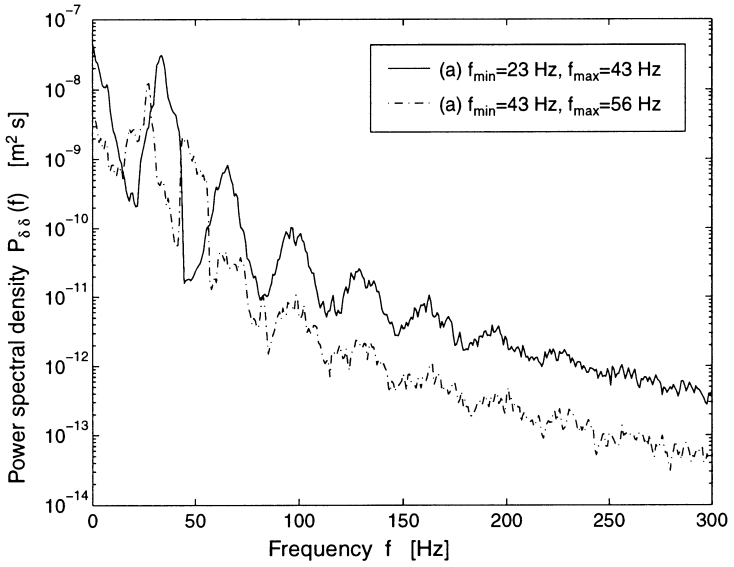


Fig. 13. Power spectral density of $\delta(t)$ to Gaussian band limited excitation with (a) $f_{\min} = 23$ Hz and $f_{\max} = 43$ Hz and (b) $f_{\min} = 43$ Hz and $f_{\max} = 56$ Hz.

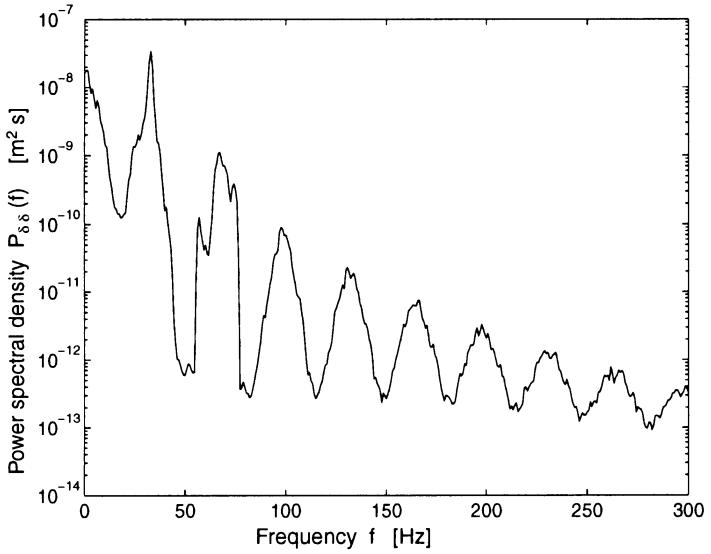


Fig. 14. Power spectral density of $\delta(t)$ for a 56–76 Hz band excitation.

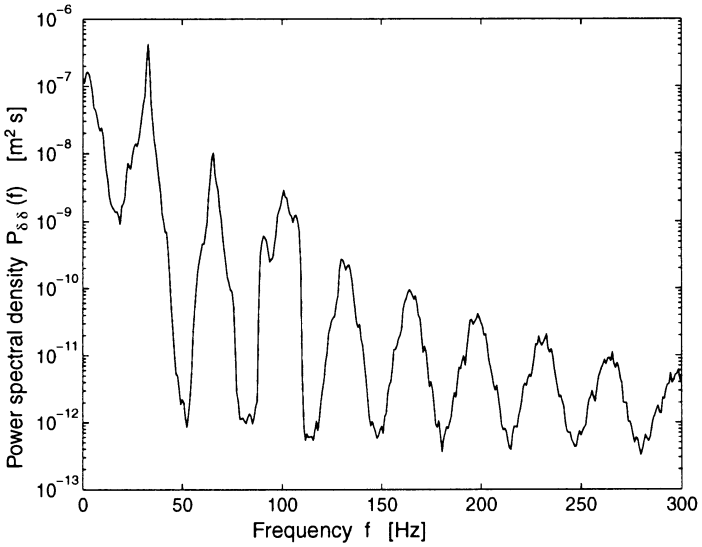


Fig. 15. Power spectral density of $\delta(t)$ for a 89–109 Hz band excitation.

convex 'valley' in the frequency band of $43\,\text{Hz} \leqslant f \leqslant 56\,\text{Hz}$. The power spectral density of the response for an excitation frequency band of $43\,\text{Hz} \leqslant f_e \leqslant 56\,\text{Hz}$ does not completely fill this convex 'valley'. This explains the fact that the response to broad banded noise excitation exhibits 'extra' frequency peaks. Moreover, a remarkable stochastic nonlinear response characteristic is revealed in Figs. 14–15, namely, the occurrence of stochastic subharmonic effects. These figures respectively show stochastic equivalents of 1/2 subharmonic and 1/3 subharmonic solutions. These stochastic equivalents of subharmonic solutions also contribute to the 'extra' frequency peaks in Fig. 12. So, there are three reasons for the extra frequency peaks in the power spectral density of the response to broad band excitation. Firstly, each frequency band in the excitation, within resonance peaks of the system, results in more frequency bands in the response, see Fig. 13. Secondly, also subharmonic effects are present. To be more specific, a $1/n$ subharmonic effect is responsible for the fact that the excitation frequency band $f_{\min} \leqslant f_e \leqslant f_{\max}$ also results in an important response in the frequency range $f_{\min}/n \leqslant f \leqslant f_{\max}/n$, see Figs 14–15. Finally, the interaction of multiple excitation frequencies will contribute energy to the multiple frequency peaks in the response.

We can distinguish another interesting nonlinear response characteristic by investigating the variance estimates $\hat{\sigma}_\delta^2$ of the response signals, see Table 1. It should be noted that the variance estimates of the previously defined excitation signals are approximately equal. It is clear that the stochastic subharmonic resonances are stronger (in terms of energy) than the stochastic harmonic resonance. Furthermore, the variance estimate of the stochastic 1/3 subharmonic solution is

Table 1. Variance estimates of the response $\delta$ to the different excitations

| $f_{\min}$–$f_{\max}$ (Hz) | 23–43 | 56–76 | 89–109 |
|---|---|---|---|
| $\hat{\sigma}_\delta^2$ (mm²) | 0.37 | 0.88 | 1.87 |

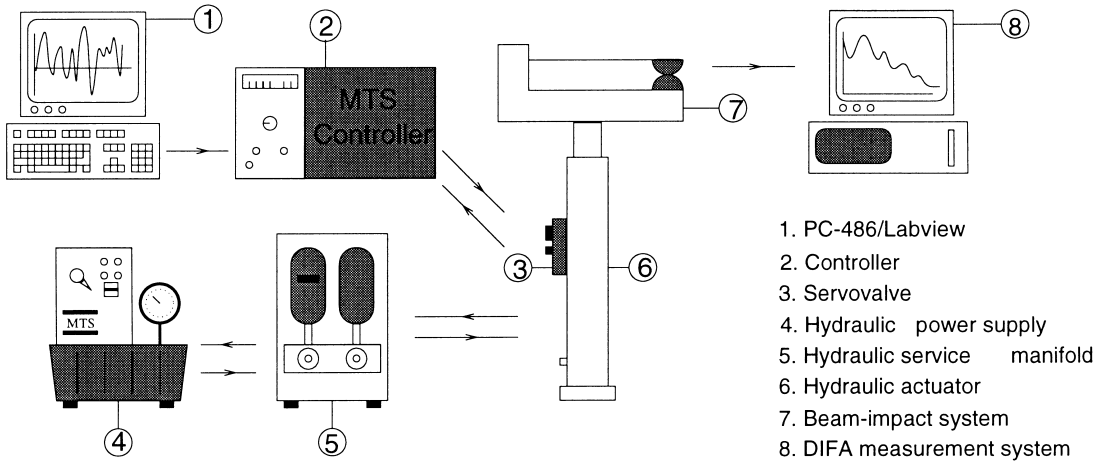


Fig. 16. The experimental set-up.

significantly higher than the variance estimate of the stochastic 1/2 subharmonic solution. These characteristics perfectly match with their periodic equivalents, see Fig. 5.

## 6. EXPERIMENTAL SET-UP

Several interesting stochastic nonlinear response characteristics were observed in the previous simulation results. In the next section, Section 7, simulation results will be validated by comparison to experimental results. The experimental set-up is presented schematically in Fig. 16. A uniformly distributed Gaussian band limited excitation signal is generated numerically using Shinozuka's method [9]. This signal is sent to a controller which controls a servo valve using feedback information from an internal displacement transducer. The servo valve provides the input for the hydraulic actuator by controlling the oil flow of the hydraulic power supply. A hydraulic service manifold connects the hydraulic power supply and the servo valve. This service manifold reduces fluctuations and snapping in the hydraulic lines during dynamic programs. All measurements are monitored using the data acquisition software package DIFA [12].

Figure 17 shows the measurement equipment mounted on the beam-impact system. A Linear Variable Differential Transformer (LVDT) measures the displacement of the rigid frame. The displacement and velocity of the beam, at the point of contact, are measured by a laser interferometer. Furthermore, the acceleration of the beam is measured by an accelerometer. Moreover, a force transducer is used to measure the force acting on the rigid frame. The rigid frame displacement measurements are used as input for the simulations described in the next section, Section 7. Consequently, we can compare the results of these simulations to the experimental results.

## 7. EXPERIMENTAL RESULTS

Several experiments were performed in order to investigate the response phenomena, observed in the former simulation results. Again, a 200 Hz (broad) band excitation was applied. The realized excitation spectrum is depicted in Fig. 18. In contrast with the signal offered to the controller, the power spectral density of the actual rigid frame displacement is clearly not

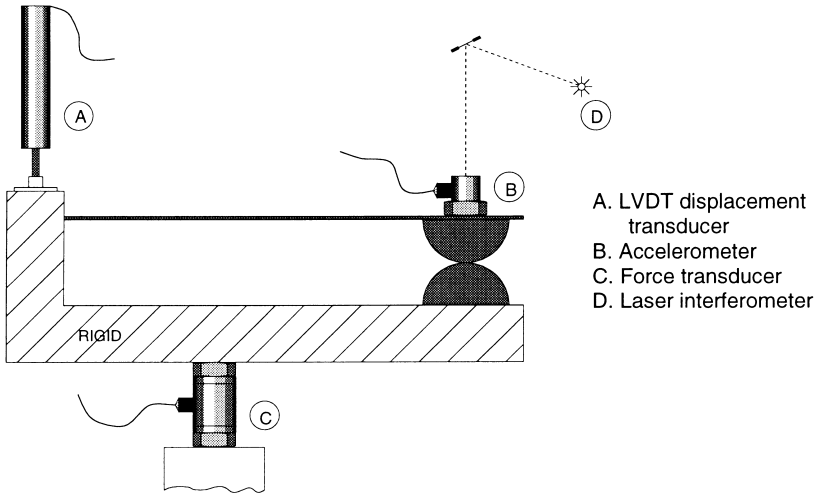


Fig. 17. The measurement equipment.

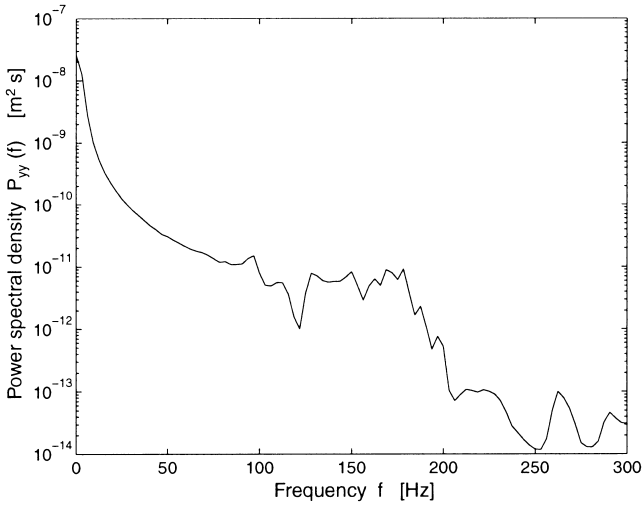


Fig. 18. Power spectral density of the 200 Hz band excitation.

uniformly distributed within the specified frequency range. This is due to the fact that the hydraulic actuator behaves like a first-order low-pass filter. Therefore, it is necessary to perform simulations with these rigid frame excitation spectra in order to be able to make appropriate comparisons between simulations and experiments.

The estimates of the probability density functions of both the excitation $y(t)$ and the response $\delta(t)$ are shown in Figs 19 and 20, respectively. In Fig. 20, the experimental results are compared to the simulation results. The experimental results clearly display the fact that the response is non-Gaussian. Both the simulated and measured power spectral densities of the response $\delta(t)$ are shown in Fig. 21. The most important response phenomena like multiple resonance peaks and the presence of a large amount of low frequency energy are clearly visible in both experimental and simulation results. However, the non-uniformity of $P_{yy}(f)$ obstructs the observation of the second characteristic. Figures 20–21 show that the experimental and numerical results correspond

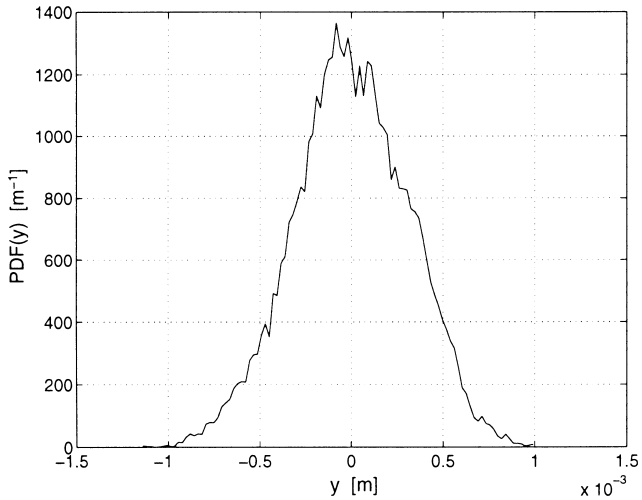


Fig. 19. Probability density function of the measured 0–200 Hz band excitation $y(t)$.

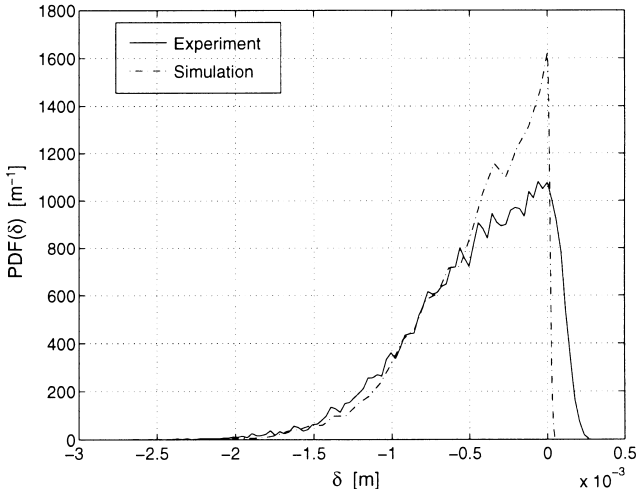


Fig. 20. Probability density function of $\delta(t)$ for a 0–200 Hz band excitation.

to a large extent. The experimental resonance peak around 120 Hz is due to the second harmonic resonance of the beam system, related to the second eigenfrequency†. Of course, this resonance peak is absent in the simulation results as a consequence of SDOF modeling.

In the experiments two narrow-band excitations were considered:

1. A limited band excitation between $f_{\min} = 23$ Hz and $f_{\max} = 43$ Hz that covers the major part of the harmonic resonance peak, see Fig. 22.
2. A limited band excitation between $f_{\min} = 56$ Hz and $f_{\max} = 76$ Hz that covers the major part of the 1/2 subharmonic resonance peak, see Fig. 24.

† In case of a nonlinear system, one cannot speak of *eigenfrequencies* of the system. However, here this terminology is used for a frequency at which the system resonates.

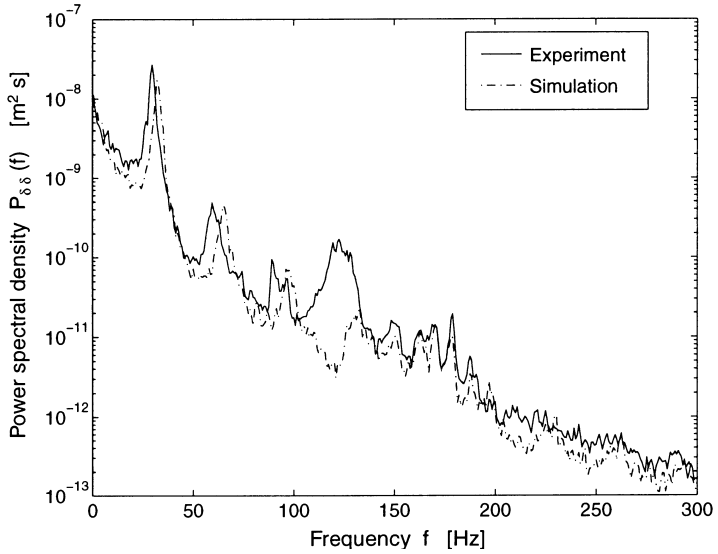


Fig. 21. Power spectral density of the response $\delta(t)$ to the 200 Hz band excitation.

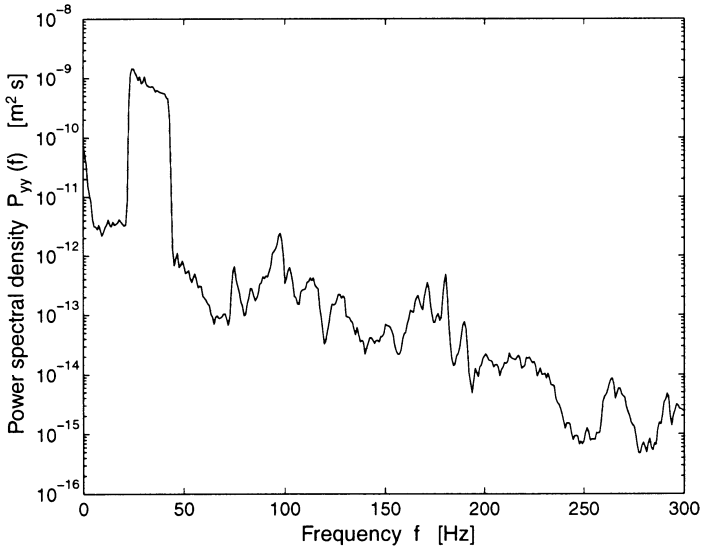


Fig. 22. Power spectral density of the measured 23–43 Hz band excitation $y(t)$.

The purpose is to find out whether the phenomena discussed in Section 3 also appear in the experiments. The spectra of the response signals $\delta(t)$ are depicted in Figs 23 and 25. Apart from the presence of the second harmonic resonance in the experiments, the simulation results match the experimental results very well. Figure 23 clearly confirms the multiple frequency property of the nonlinear response experimentally. Furthermore, a stochastic 1/2 subharmonic effect is also found in the experiments, see Fig. 25.

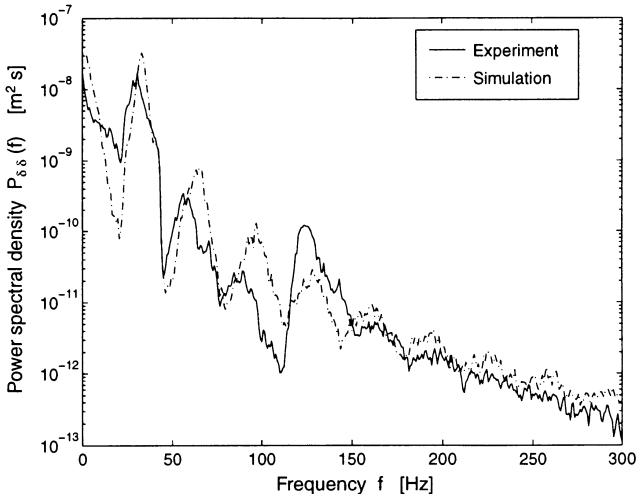


Fig. 23. Power spectral density of the response $\delta(t)$ to the 56–76 Hz band excitation $y(t)$.

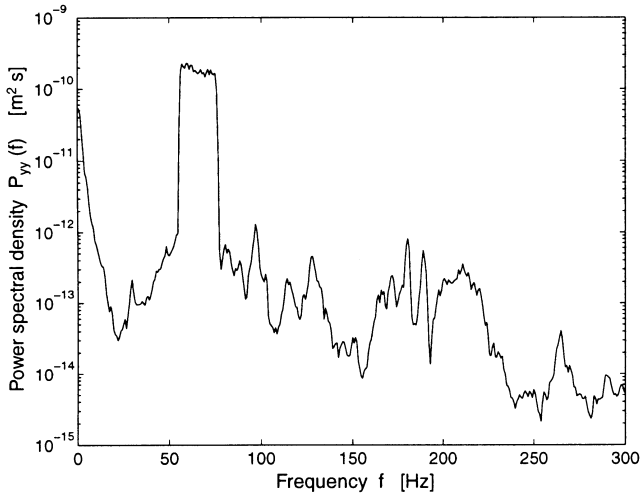


Fig. 24. Power spectral density of the measured 56–76 Hz band excitation $y(t)$.

## 8. CONCLUSIONS

We have applied Gaussian band limited excitations to a strongly nonlinear impacting system. The derived nonlinear model is SDOF. Many interesting, specifically nonlinear, stochastic response phenomena have been investigated both numerically as well as experimentally. Both broad- and narrow-band excitations are applied in order to discriminate the origin of certain response characteristics in the frequency domain. We have focussed on the investigation of frequency domain characteristics, because in literature little attention has been paid to this subject.

Nonlinear stochastic phenomena like multiple resonance peaks and a high-energy low-frequency response content are found applying broad-band excitations. The origin of the multiple resonance frequencies is illuminated by investigating the system's response to narrow-band

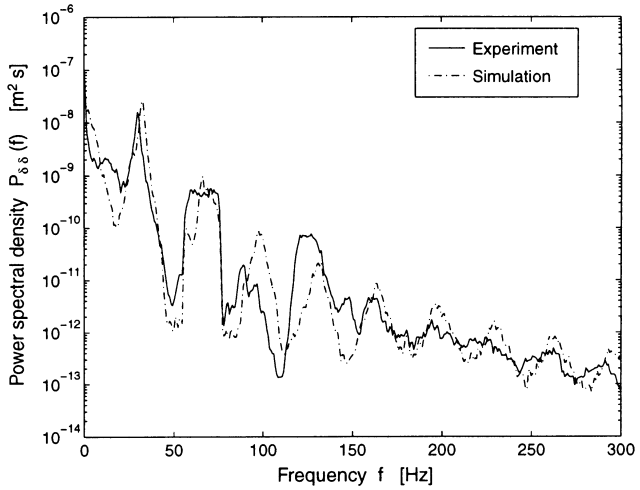


Fig. 25. Power spectral density of the response $\delta(t)$ to the 23–43 Hz band excitation $y(t)$.

excitations covering harmonic and subharmonic resonance regions. Stochastic equivalents of harmonic and subharmonic solutions are found. With respect to all these response characteristics, the numerical and experimental results agree to large extent. The observed phenomena can also be found in systems with other one-sided nonlinearities [13]. Therefore, these characteristics can give insight in the nonlinear stochastic behaviour of a large class of nonlinear dynamic systems.

Future research will involve the extension of the model to include higher modes of the beam. This extension will improve the response characteristics around the second harmonic resonance frequency. Moreover, such a multi-degree-of-freedom model might also describe the system better for lower frequencies, because these higher modes affect the behaviour in the lower frequency range for periodic excitations, see Fig. 5.

## REFERENCES

1. Fey, R., Steady-state behaviour of reduced dynamic systems with local nonlinearities. Ph.D thesis, Eindhoven University of Technology, The Netherlands, 1992.
2. Fey, R., Van Campen, D., De Kraker, A., Long term structural dynamics of mechanical systems with local nonlinearities. *Trans. ASME, J. Vibration and Acoustics*, 1996, **118(2),** 147–153, Also publ. in *Proc. Winter Annual Meeting ASME*, Anaheim (Calif., USA), 8–13 November, DE-Vol. 50, AMD-Vol. 44, eds. R. A. Ibrahim and N. S. Namachchivaya. 1992, pp. 159–167.
3. Van de Vorst, E., Long term dynamics and stabilization of nonlinear mechanical systems. Ph.D. thesis, Eindhoven University of Technology, The Netherlands, 1996.
4. Van Campen, D., De Kraker, A., Fey, R., Van de Vorst, E., Van der Spek, J., Long-term dynamics of nonlinear mdof engineering systems. *Chaos, Solitons and Fractals*, 1997, **8(4),** 455–477, Special issue on Nonlinearities in Mechanical Engineering.
5. Hertz, H., *Gesammelte Werke*, Vol. 1: Schriften Vermischten Inhalts, J. A. Barth, Leipzig, Germany (in German), 1895.
6. Goldsmith, W., *Impact*: *The Theory and Physical Behaviour of Colliding Solids*. E. Arnold Ltd., London, 1960.
7. Roozen-Kroon, P., Structural optimization of bells. Ph.D. thesis, Eindhoven University of Technology, The Netherlands, 1992.
8. Lankarani, H., Nikravesh, P., Continuous contact force models for impact analysis in multibody systems. *Nonlinear Dynamics*, 1994, **5,** 193–207.
9. Shinozuka, M., Monte Carlo solution of structural dynamics. *Computers and Structures*, 1972, **2,** 855–874.

10. Yang, J.-N., Simulation of random envelope processes. *Journal of Sound and Vibration*, 1972, **21(1),** 73–85.
11. Hénon, M., On the numerical computation of Poincaré maps. *Journal of Applied Mechanics*, 1982, **47,** 931–939.
12. DIFA, *FA*100 *User Manual*. DIFA Measuring Systems, Breda, The Netherlands, 1992.
13. Van de Wouw, N., De Kraker, A. and Van Campen, D., Nonlinear phenomena in a stochastically excited dynamic system. In *Proc*. 1997 *ASME Int*. *Mechanical Engineering Congress and Exposition*, *Dallas* (*USA*), DE-Vol. 95, AMD-Vol. 223, 16–21 Nov. 1997, eds. W. C. Xie, N. S. Namachchivaya and O. M. O'Reilly. 1997, pp. 151–158.